Received: 25 April 2023 | Revised: 24 July 2023 | Accepted: 26 July 2023

DOI: 10.1002/ese3.1536

ORIGINAL ARTICLE

Performance analysis of multistage high-temperature heat pump cycle

Seon Tae Kim | **Robert Hegner** | **Göksel Özuylasi** | **Panagiotis Stathopoulos** | **Eberhard Nicke**

Institute of Low-Carbon Industrial Process, German Aerospace Center (DLR), Mandau-Höfe, Zittau, Germany

Correspondence
Seon Tae Kim, Institute of Low-Carbon Industrial Processes, German Aerospace Center (DLR), Mandau-Höfe, Haus 9, Äußere Oybiner Straße 14/16, Zittau 02763, Germany.
Email: seon.kim@dlr.de

Abstract

High-temperature heat pumps (HTHPs) that can supply heat at temperatures at and above 200°C have the potential to increase energy efficiency and decrease carbon dioxide (CO_2) emissions in industrial processes. In this study, three reversed Rankine cycles using water vapor (R-718) as the working medium, with different intercooling strategies, were proposed and their performance has been investigated. The thermodynamic performance was estimated under different operating conditions, and the optimal pressure ratio (PR) between compression stages was found to be where both compressors had the same PR. The thermodynamic efficiency, φ, and exergy efficiency, η_{exergy}, were also analyzed at the optimum PR. The cycles that employed an intercooler between the first and second compression stages (IC cycles) showed higher φ and η_{exergy} values compared with the spray-injection cycle. Among the IC cycles, the IC-in cycle, with an inward flow direction of heat sink to the IC, demonstrated higher efficiency and deliverable temperature, $T_{sink\ out}$, than the spray-injection and IC-out cycles. To assess the practical impact of the HTHP cycles on industrial CO_2 reduction, the PR for each stage was limited to 2.5. Theoretically, the IC-in cycle could achieve a coefficient of performance of 5.86 with a $T_{sink\ out}$ of 200°C or higher when T_{evap} and T_{cond} were at 90°C and 150°C, respectively. Additionally, the study demonstrated that the proposed HTHP system has the potential to reduce CO_2 emissions by 8.1% in 2030 for industrial heat supply at temperature up to 200°C, by replacing existing industrial fossil boilers with high-efficiency HTHP.

KEYWORDS

high-temperature heat pump, industrial processes, multistage vapor compression cycle, R-718 (water), thermodynamic analysis

1 | INTRODUCTION

For the past few decades, global greenhouse gas (GHG) emissions have been increasing steadily and finally reached 51,199 Mt CO_2-eq of GHG in 2018 excluding agriculture, forestry, and other land uses (AFOLU). Specifically, carbon dioxide (CO_2) accounts for over 73%, of total GHG emissions.[1] Among all sectors, the energy sector has the largest share of GHG emissions, followed by the industrial sector, which is responsible for 34.8% of global GHG emissions. With the constantly increasing decarbonization of the energy sector through renewable generation, the industrial sector is becoming increasingly important for reaching the climate goals of the European Union (EU).[2,3]

In 2019, 120,944 PJ were consumed in the industrial sector, and the fossil fuels share was over 58% (70,544 PJ).[4] While the EU has been concentrating on reducing energy consumption per unit for many years, the total energy usage did not greatly decrease.[5,6] Heat supply is the dominant source of emissions in the industrial sector (73% of final energy consuming in 2015). Heat supply temperatures correlate with specific branches and the respective processes; for example, the largest share of heat in the food industry is delivered at temperatures below 100°C, between 100°C and 500°C for the chemical industry, and above 500°C for iron and steel production, respectively.[7,8] In addition, process heat below 500°C is generally supplied in the form of steam and hot water, while process heat above 500°C is mainly connected to industrial furnaces.[9]

Waste heat recovery is an excellent way to improve the energy efficiency of industrial processes.[10–12] Apart from power generation from high-temperature waste heat, an efficient option to upgrade and recycle waste heat is with industrial heat pumps and their combination with other renewable energy sources (solar, geothermal, and so on). Heat pumps are used in domestic applications and are currently a niche application in industrial processes. However, electrification is eventually required for heat supply decarbonization, thus making industrial heat pumps a core element in any decarbonization strategy, both in large industries and small and midsize enterprises.[13–18] Many industrial heat pump systems have been developed with technological advancements in the working media, compressors, heat exchangers, and control concepts. However, most commercial heat pumps can deliver heat at a maximum temperature of 150°C, mainly because of component limitations.[19,20] Despite this shortcoming, there are still several research and development efforts to push the sink temperature of industrial heat pumps to 200–250°C, and thus extending their availability for a larger proportion of industrial processes.[21,22]

Selecting an appropriate working medium is also important for the development of high-temperature heat pump (HTHP) for industrial processes. Generally, working media with a global warming potential (GWP) of less than 150 are considered by the community, with the main focus being on using natural working media,[23–27] such as Water (R-718). Water has zero GWP and ozone depletion potential, and it is also easily available, nontoxic, nonflammable, nonexplosive, and chemically stable. As a working medium at high temperatures, water exhibits distinctive thermodynamic properties. Because of its high critical temperature (373.95°C), water is suitable for HTHP working at temperatures between 200°C and 250°C. A further advantage of water in heat pump applications is its high evaporation enthalpy (~2256 kJ/kg at 1 bar at 100°C).

The current work focuses on three methods to integrate the heat sink into the cycle of a two-stage water vapor reversed Rankine HTHP. Parameter studies are performed to find the optimum design solutions for each integration strategy and to compare the strategies with each other. To the knowledge of the authors, this is the first time, that the studied cycle architectures and integration concepts have been studied in the open literature. Furthermore, this study will serve as valuable fundamental research data for the development of the industrial HTHP system by our group, the DLR Institute of Low-Carbon Industrial Processes. The HTHP targets a higher heat sink temperature, above 150°C, compare to other conventional heat pump systems, and the practical validation will be carried out while the system is in operation.

2 | HEAT SINK INTEGRATION CONCEPTS AND MODELING AND ANALYSIS METHODS

2.1 | Heat sink integration concepts

The three studied concepts to integrate the heat sink in a water vapor compression cycle are presented schematically and on the corresponding *T*–*S* diagrams in Figure 1. All cycles employ intercooling between the first and second compression stages to reduce the degree of superheating at the inlet of the second compression stage and also its efficiency. The target sink temperature is defined by the outlet pressure of the second compression stage. The intermediate pressure, the pressure between the two compression stages, is typically determined by the geometric mean of the total pressure ratio (PR) of the cycle, PR between condenser and evaporator.[28] The current work focuses on three integration

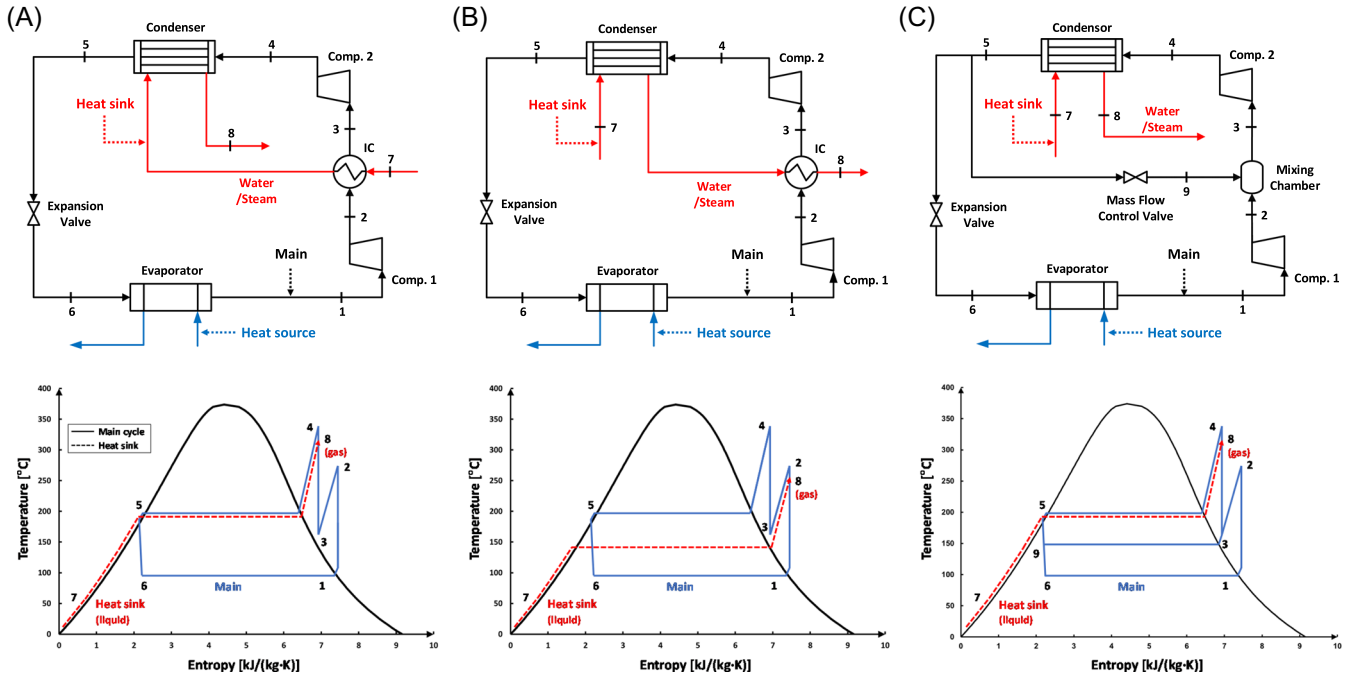

FIGURE 1 Schematic and ideal *T*–*S* diagrams of the heat pump cycles studied: (A) IC-in, (B) IC-out, and (C) spray injection. IC, intercooler.

strategies of the heat sink in the heat pump cycle. The first two options, integrate the heat sink in the intercooler (IC) and are presented in Figure 1A,B. The IC cycles differ in the direction of the heat sink flow against the IC on the main heat pump cycle (IC-in and IC-out). The last option is a typical spray-injection cycle, Figure 1C with the heat sink solely connected to the condenser of the heat pump.

2.2 | Simulation process and methodology

The proposed HTHP cycles were modeled with EBSILON Professional 15 using IAPW-IF97 as the standard thermodynamic fluid library of water steam.[29] The software is a steady-state simulation tool and is widely used in industry and research.[30,31] The flowchart in Figure 2 depicts the calculation process of the multistage HTHP cycle, and the overall specifications of the HTHP model are provided in Table 1. The cumulative power consumption of the two compressors was fixed at 120 kW for all simulations. The pinch point between the main and secondary flows in the evaporator and condenser was assumed to be 10 K. The working medium temperature after the evaporator was set to 10 K above the saturation temperature and it had 10 K subcooling at the outlet of the condenser, points 1 and 5 in Figure 1. In addition, the pressure drop in the heat exchangers was neglected for simplicity. With regard to the heat sink flow, the inlet temperature of the heat sink was 15°C in the liquid state, point 7 in Figure 1, and pressure, P_{sink}, was adjusted based on the pressure of the main flow at the end of the heat sink flow for heat exchange.

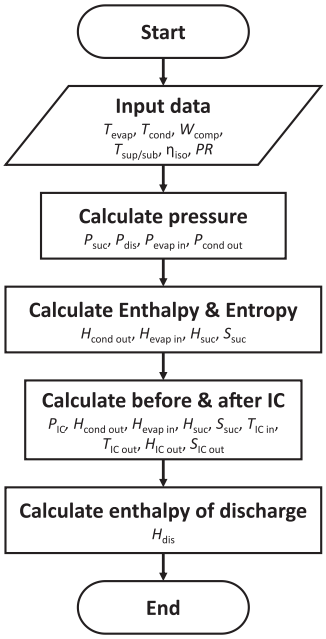

FIGURE 2 Flowchart of the calculation of multistage HTHP cycle. HTHP, high-temperature heat pump; IC, intercooler.

TABLE 1 Specifications of the considered HTHP cycle.

Category	Items	Symbol	Value/comments
Main cycle	Compressors power consumption	W_{comp}	120 kW
	Superheat/subcooling	$T_{sup/sub}$	10 K
	Isentropic efficiency of compressor	η_{iso}	0.89
Heat sink	Inlet temperature	$T_{sink\ in}$	15°C
	Pinch point temperature difference	$T_{sink\ out}$	$T_{main} - T_{sink\ out} = 10$ K
	Pressure	P_{sink}	$P_{sink} = P_{main}$ at the end of heat sink flow

Abbreviation: HTHP, high-temperature heat pump.

TABLE 2 Variable parameters for HTHP cycle simulation.

Parameter	Symbol	Value/comments
Evaporation temperature	T_{evap}	60–110°C
Condensation temperature	T_{cond}	150–250°C
Temperature increment	ΔT	5 K
Pressure increment	ΔP	0.5 bar

Abbreviation: HTHP, high-temperature heat pump.

The performance of the three different multistage cycles was studied and compared by varying the evaporation and condensation temperatures. Additionally, the intermediate pressure between the first and second compressor stages, P_{int}, was also adjusted, as shown in Table 2. The effect of these changes on the heat sink flow (i.e., change in mass flow rate), the coefficient of performance (COP), the thermodynamic efficiency, φ, and exergy efficiency, η_{exergy}, were then analyzed. The evaporation temperature was varied from 60°C to 110°C, while the condensation temperature was changed from 150°C to 250°C. The overall PR of the two compression stages was determined based on the temperature conditions, and the PR for each compression stage was adjusted sequentially during simulation. The increment of the evaporation and condensation temperature conditions was 5 K, and the intermediate pressure was varied by 0.5 bar each time. The mass flow rate of the main cycle, m_{main}, was adjusted according to the total power consumption of two compressors, and the mass flow rate of heat sink, m_{sink}, was controlled to satisfy the temperature constraints, T_{sub} after condenser and T_{sup} after IC of IC cycles. The injection mass flow, m_{inj}, for the spray-injection cycle, which is split from the main flow, was also determined to maintain a 10 K superheat before entering the second compression stage.

2.3 | Thermodynamic analysis methods

2.3.1 | Energy and thermodynamic efficiencies

The COP is the first parameter used to evaluate heat pump performance. The COP is the ratio of the useful heat transferred in the heat sink, Q_{sink}, to the power consumed by the compressors, W_{comp}, Equation (1).

$$\mathrm{COP} = \frac{Q_{sink}}{W_{comp}}. \tag{1}$$

In addition, the thermodynamic efficiency, φ, was introduced to compare the system performance with that of an ideal cycle, Equation (2). The Carnot efficiency, COP_{carnot}, is the maximum energy efficiency of an ideal process converting power to heating between two different temperatures, T_L and T_H, Equation (3).[32]

$$\varphi = \frac{\mathrm{COP}}{\mathrm{COP}_{carnot}}, \tag{2}$$

$$\mathrm{COP}_{carnot} = \frac{T_H}{T_H - T_L}. \tag{3}$$

2.3.2 | Exergetic efficiency

In comparison with conventional energy analysis, exergy analysis can quantitatively characterize and localize thermodynamic losses in a process, and define the subprocesses that require most attention. The specific exergy, ε, the difference between the flow availability of a stream and that of the same stream at its restricted dead state, is given by Equation (4) when ignoring chemical, potential, and kinetic exergy terms.[33]

$$\varepsilon = (h - T_0 s) - (h_0 - T_0 s_0) = (h - h_0) - T_0(s - s_0), \tag{4}$$

where h_0 and s_0 are the enthalpy and entropy values of the working medium at the reference states, $P_0 = 1$ atm, $T_0 = 25$°C (298.15 K). The exergy of heat, E_Q, that

contains heat, Q, at temperature, T, is obtained using Equation (5), and the values were obtained from the main cycle. The exergy efficiency, η_{exergy}, is defined as the ratio of the total outgoing exergy, E_{out}, to the total incoming exergy, E_{in}, of the heat pump system, Equation (6).

$$E_Q = Q \cdot \left(1 - \frac{T_0}{T}\right), \tag{5}$$

$$\eta_{exergy} = E_{out}/E_{in}. \tag{6}$$

To investigate the effect of cycle architecture on performance, an exergy analysis was carried out. The total exergy input, E_{in}, of the heat pumps is given by Equation (7). Because the number of utilizing heat exchangers is different between IC cycles and spray-injection cycles, total outgoing exergy, E_{out}, for both cycles are defined by Equations (8) and (9), respectively.

$$E_{in} = W + (1 - T_0/T_{evap\,in}) \cdot Q_{evap}, \tag{7}$$

$$E_{out\,IC} = (1 - T_0/T_{cond\,out}) \cdot Q_{cond} + (1 - T_0/T_{m\,IC}) \cdot Q_{IC}, \tag{8}$$

$$E_{out\,inj} = (1 - T_0/T_{cond\,out}) \cdot Q_{cond}, \tag{9}$$

where T_m is the logarithmic mean temperature difference (LMTD) and it was adopted to calculate the representative temperature in an IC. The main flow in the IC is not associated with the phase change, and the LMTD method can represent nonlinear temperature changes across the heat exchanger from entrance to exit effectively.

$$T_m = (T_{IC\,in} - T_{IC\,out})/\ln\left(\frac{T_{IC\,in}}{T_{IC\,out}}\right). \tag{10}$$

3 | RESULTS AND DISCUSSION

3.1 | Simulation results of multistage water vapor compression cycle

In this section, the performance of the proposed HTHP cycles is evaluated for different combinations of evaporation temperature, T_{evap}, condensation temperature, T_{cond}, and intermediate pressure, P_{int}. The mass flow rate and outlet temperature of heat sink, m_{sink} and $T_{sink\ out}$, are investigated initially as these parameters are directly related to the heat demand. To evaluate the impact on cycle performance, the pressure ratio, $PR = PR_1/PR_2$, between the first and second compression stages is varied under specified evaporation and condensation temperature conditions, T_{evap} and T_{cond}, as outlined in Table 2.

To satisfy the cycle constraint that maintains a temperature difference of 10 K between the main cycle and heat sink, $T_{main} - T_{sink\ out} = 10$ K, it is necessary to adjust the mass flow rate of heat sink. This parameter is affected by the main cycle temperature, discharge temperature for IC-in and spray-injection cycles, and intermediate temperature for IC-out cycle. The results show that the m_{sink} of the IC-in and spray-injection cycles increase with PR, while the value of the IC-out cycle decreases for all temperature conditions. From Figure 3A,B, it was observed that the mass flow rate of the heat sink, m_{sink}, is strongly correlated with the temperature lift value, $T_{lift} = T_{cond} - T_{evap}$. Overall, the mass flow rate increases as T_{lift} decreases, with no specific observed from varying T_{evap} and T_{cond}. For instance, the cycle with the lowest T_{lift}, 100–150 in Figure 3A, exhibits the highest m_{sink}, while graphs with $T_{lift} = 60$°C, 100–160 in Figure 3A and 90–150 in Figure 3B, show similar m_{sink} values despite representing different temperature conditions. In particular, the spray-injection cycle has a slightly lower m_{sink} than the IC-in cycle, because the heat sink flow passes only through the condenser, to control the superheating degree of the main cycle.

The heat sink outlet temperature, $T_{sink\ out}$, shows a similar trend to the mass flow rate, Figure 3C,D. The IC-in and spray-injection cycles have the same outlet temperature, while the IC-out cycle has different results. The temperature of the IC-out cycle increases with PR because this value is linked to the intermediate temperature, T_{int}, while the $T_{sink\ out}$ of the IC-in and spray-injection cycles decrease. The temperature lift condition also has more effect on $T_{sink\ out}$ than changes in T_{evap} and T_{cond}. $T_{sink\ out}$ value increase with increasing T_{lift} contrary to the case of m_{sink}. Especially, all of the proposed HTHP cycles exhibit a heat sink outlet temperature that exceeds 200°C, which is the target of this study, except for IC-out cycle at low PR.

Figure 4 depicts the relationship between COP and PR between the first and second compression stages for different temperature conditions. The results show that as temperature lift values decrease, COP values increase, similar to the behavior observed for m_{sink}. Additionally, it was found that cycles with the same T_{lift} exhibit a similar range of COP, and COP values are more strongly influenced by temperature lift values than by evaporation and condensation temperature.

The IC cycles demonstrate higher COP than the spray-injection cycle because of their ability to utilize two

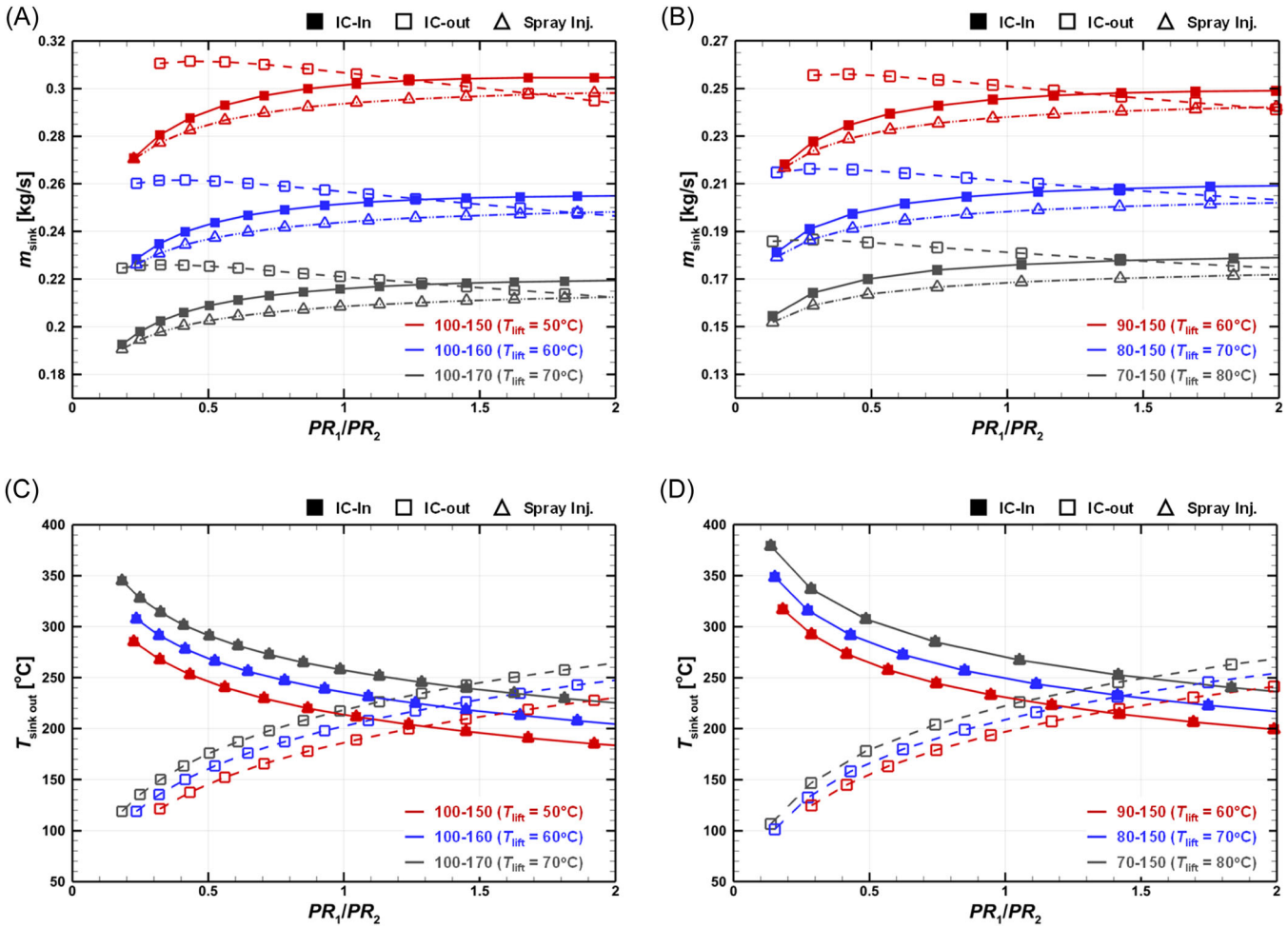

FIGURE 3 m_{sink} and $T_{sink\ out}$ changes by pressure ratio, PR_1/PR_2: (A, C) with fixed evaporation temperature, T_{evap}, and (B, D) with fixed condensation temperature, T_{cond}. IC, intercooler; PR, pressure ratio.

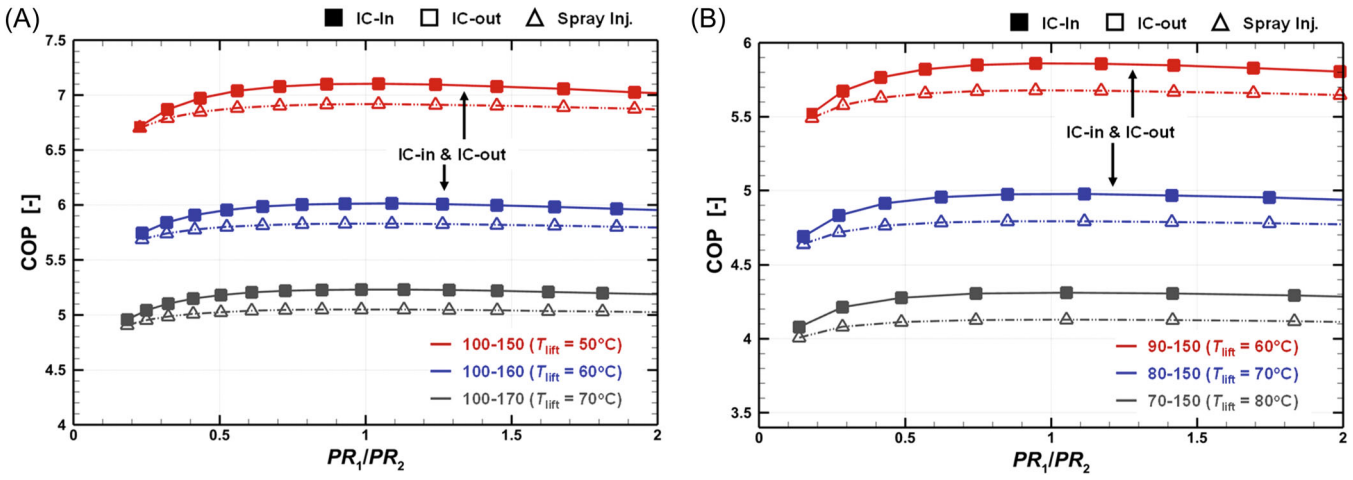

FIGURE 4 COP changes by pressure ratio, PR_1/PR_2: (A) with fixed evaporation temperature, T_{evap}, and (B) with fixed condensation temperature, T_{cond}. COP, coefficient of performance; IC, intercooler; PR, pressure ratio.

heat exchangers. Detailed analysis revealed that the IC-in cycle has the same $T_{\text{sink out}}$ but higher m_{sink} across the entire range of PR due to its architectural advantages of using an IC and condenser. Similarly, the IC-out cycle has higher m_{sink} and $T_{\text{sink out}}$ at low and high PR, respectively, as shown in Figure 3. These results suggest that the use of two heat exchangers and architectural advantages of IC-in and IC-out cycles led to a higher COP for both cycles.

The COP values show a rapid increase when the first compression stage has a low, $PR_1/PR_2 < 0.5$. The highest COP values were achieved when the PR of both compressors were equal, $PR_1/PR_2 = 1.0$, under all temperature conditions.

3.2 | Thermodynamic performance at the optimized PR

On the basis of the results in Section 3.1, where the highest COP was confirmed when both compressors had the same pressure ratio, $PR_1/PR_2 = 1.0$, was selected as the optimized PR for the HTHP cycles. Therefore, the thermodynamic performances of the HTHP cycles at the optimized PR were evaluated in this section.

Figure 5A illustrates the optimized COP change with respect to the evaporation and condensation temperatures ($T_{\text{evap}} = 60$–$110°C$, $T_{\text{cond}} = 150$–$250°C$). As the temperature lift decreases, COP values increase exponentially from around 1.94 to 8.97. Both IC-in and IC-out cycles exhibit the same COP as shown in Figure 4A. Although IC-in has a higher $T_{\text{sink out}}$ value than the IC-out cycle at optimized PR as shown in Figure 3C,D, the IC-out cycle has a higher m_{sink} at that point as shown in Figure 3A,B. On the other hand, the spray-injection cycle shows 2.07%–7.68% lower COP than the IC cycles. Basically, the spray-injection cycle has a higher mass flow rate on the main cycle, m_{main}, than IC cycles at the same temperature conditions because a certain amount of m_{main} should be used for injection flow to cool down T_{int} to near the condensation temperature. However, after splitting with injection flow, the spray-injection cycle has a lower mass flow rate for evaporation, m_{evap}, that exchange the thermal energy with heat source. Additionally, m_{sink} is low owing to the architectural features of the spray-injection cycle. These low values of m_{evap} and m_{sink} result in a low COP for the spray-injection cycle.

The result of the exergy efficiency, η_{exergy}, showed a similar trend as the COP analysis, Figure 5B. The IC cycles had the same η_{exergy}, and these values, which gradually increased with decreasing T_{lift}. Consistent with the COP analysis at an optimized PR, the IC cycles had η_{exergy} values ranging from 0.81 to 0.96, while the injection cycle had 0.88%–6.75% lower values. Further analysis revealed that the spray-injection cycle had a lower m_{evap} resulting in 1.5%–2.7% lower exergy input, E_{in} in Equation (7), compared with the IC cycles. Regarding the exergy out, E_{out} in Equations (8) and (9), the spray-injection cycle had a higher Q_{cond} value than the IC cycles due to the higher m_{main} in the condenser. However, accounting for the thermal energy exchange in the IC, Q_{IC}, the IC cycles exhibited 2.4%–8.2% higher E_{out}. In conclusion, the results indicate that the IC cycles are more efficient in terms of exergy efficiency than the spray-injection cycle under the studied conditions.

Figure 6 shows the variation in thermodynamic efficiency, φ, which is the ratio of the actual COP to the Carnot COP, with respect to the T_{evap}, T_{cond}, and T_{lift} at the optimized pressure ratio, $PR_1/PR_2 = 1.0$. Generally, it can be observed that the value of φ increases with T_{evap}, Figure 6A, and it decreases with increasing T_{cond} or T_{lift}, Figure 6B,C. Both IC-in and IC-out cycles exhibit the same φ, while the spray-injection cycle has

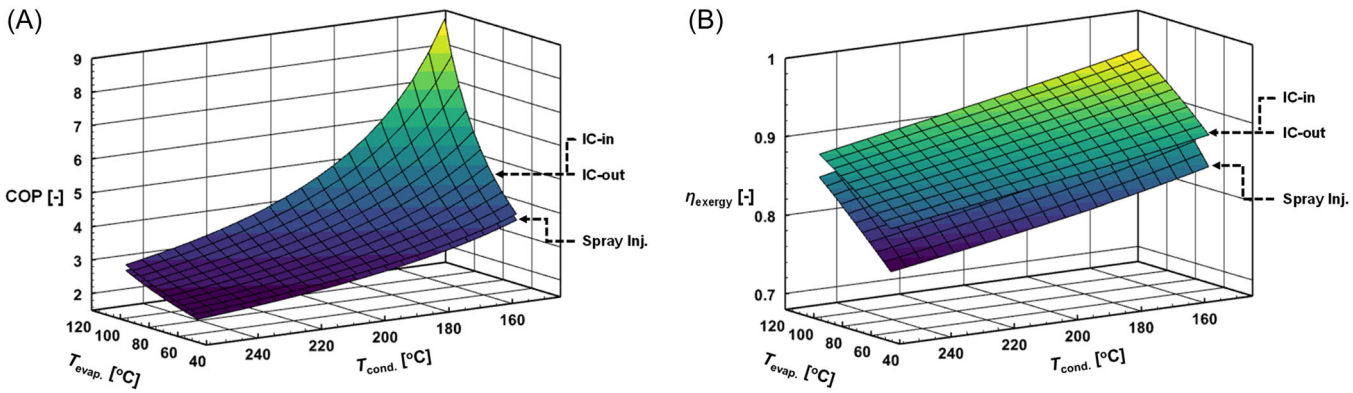

FIGURE 5 Performance of the HTHP cycles at optimized pressure ratio: (A) COP and (B) η_{exergy}. COP, coefficient of performance; HTHP, high-temperature heat pump; IC, intercooler.

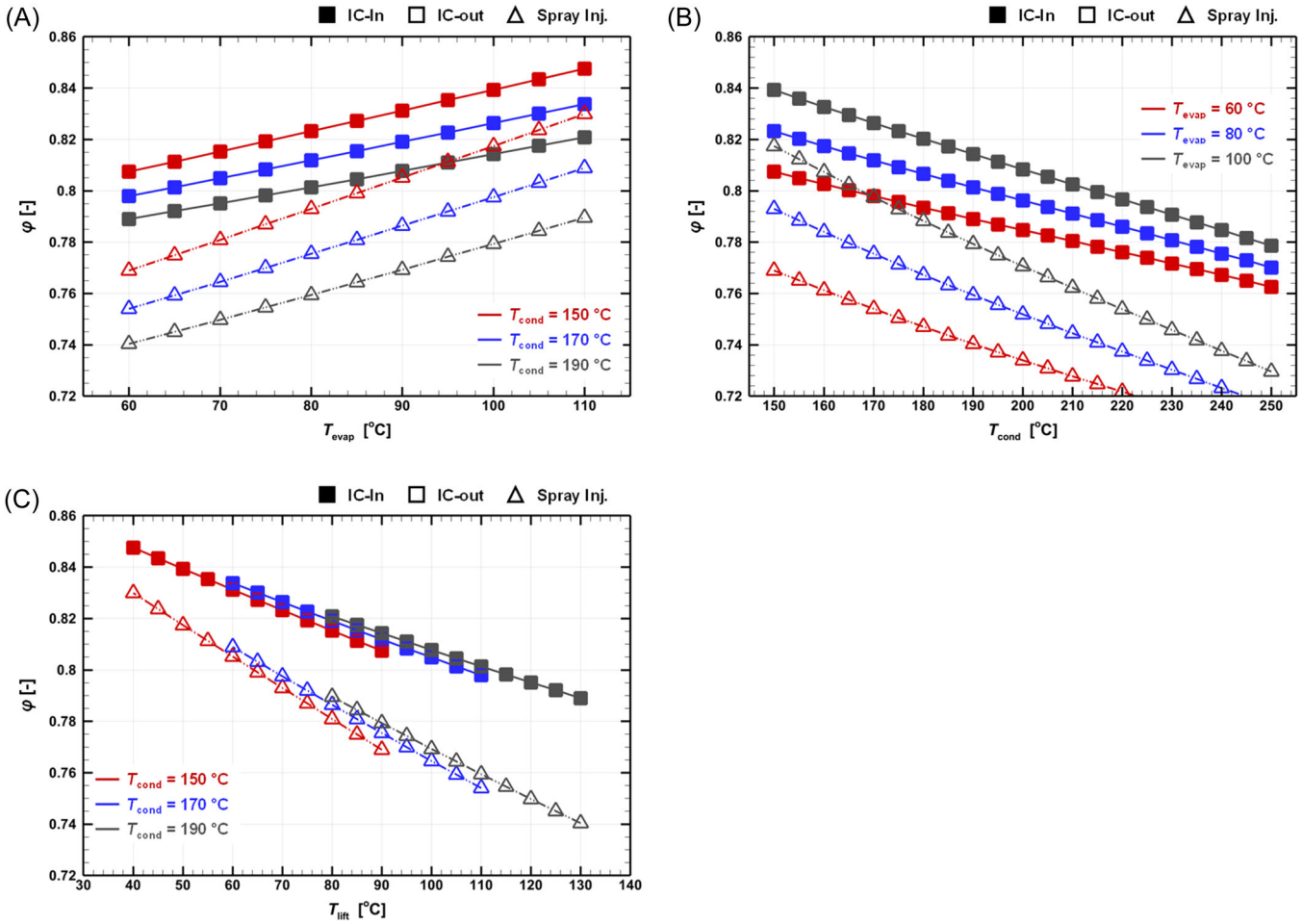

FIGURE 6 Thermodynamic efficiency, φ, changes according to (A) evaporation temperature, T_{evap}, (B) condensation temperature, T_{cond}, and (C) temperature lift, T_{lift}. IC, intercooler.

a lower φ than the IC cycles due to its different architectural characteristics as previously explained in Section 3.1.

The difference in φ between the IC and spray-injection cycles varied with temperature conditions. When T_{evap} is 60°C, the IC cycle had a φ of 0.79–0.81, while the spray-injection cycle had a φ that was 4.76%–6.17% lower, 0.74–0.77. As T_{evap} increased to 110°C, the difference in φ decreased to 2.07%–3.82%; IC cycles had a φ of 0.82–0.85 and the spray-injection cycle had a φ of 0.79–0.83, Figure 6A. When T_{evap} has fixed values, the discrepancy between the IC and spray-injection cycles increased with T_{cond} as shown in Figure 6B. Specifically, the difference between the IC and spray injection increased from 2.60%–4.76% to 6.28%–7.68% as T_{cond} increased from 150°C to 250°C. It is important to note that T_{evap} and T_{cond} have different impacts on thermodynamic efficiency; increasing T_{evap} has a positive impact, while increasing T_{cond} results in a decline in φ. In other words, the thermodynamic efficiency value is dependent on T_{lift}.

Figure 6C comprehensively presents the results of the above mentioned φ analysis. It is observed that not only does φ decreases with T_{lift}, but the discrepancy between IC and spray-injection cycles are also increases from 2.70% to 6.17% as T_{lift} changes from 40°C to 130°C. This change in discrepancy comes from the variation in the ratio of m_{inj} to m_{main} for the spray-injection cycle. Similar to the other cycles, the main mass flow rate, m_{main}, of the spray-injection cycle decreases significantly with increasing T_{lift}. However, m_{inj} does not change significantly with increasing T_{lift}. This is because while the higher T_{lift} cycle has low m_{main}, the required heat for cooling at intermediate stage increases with T_{lift}. Therefore, as T_{lift} increases, the ratio of m_{inj} that is not involved in heat exchange with the heat source at evaporator relatively. This increase in the m_{inj} ratio induces a further decline in the φ of the spray-injection cycle compared with the IC cycles.

The change in exergy efficiency, η_{exergy}, showed a similar tendency to that of the thermodynamic efficiency, φ, Figure 7. The IC cycles had the same η_{exergy}, and the

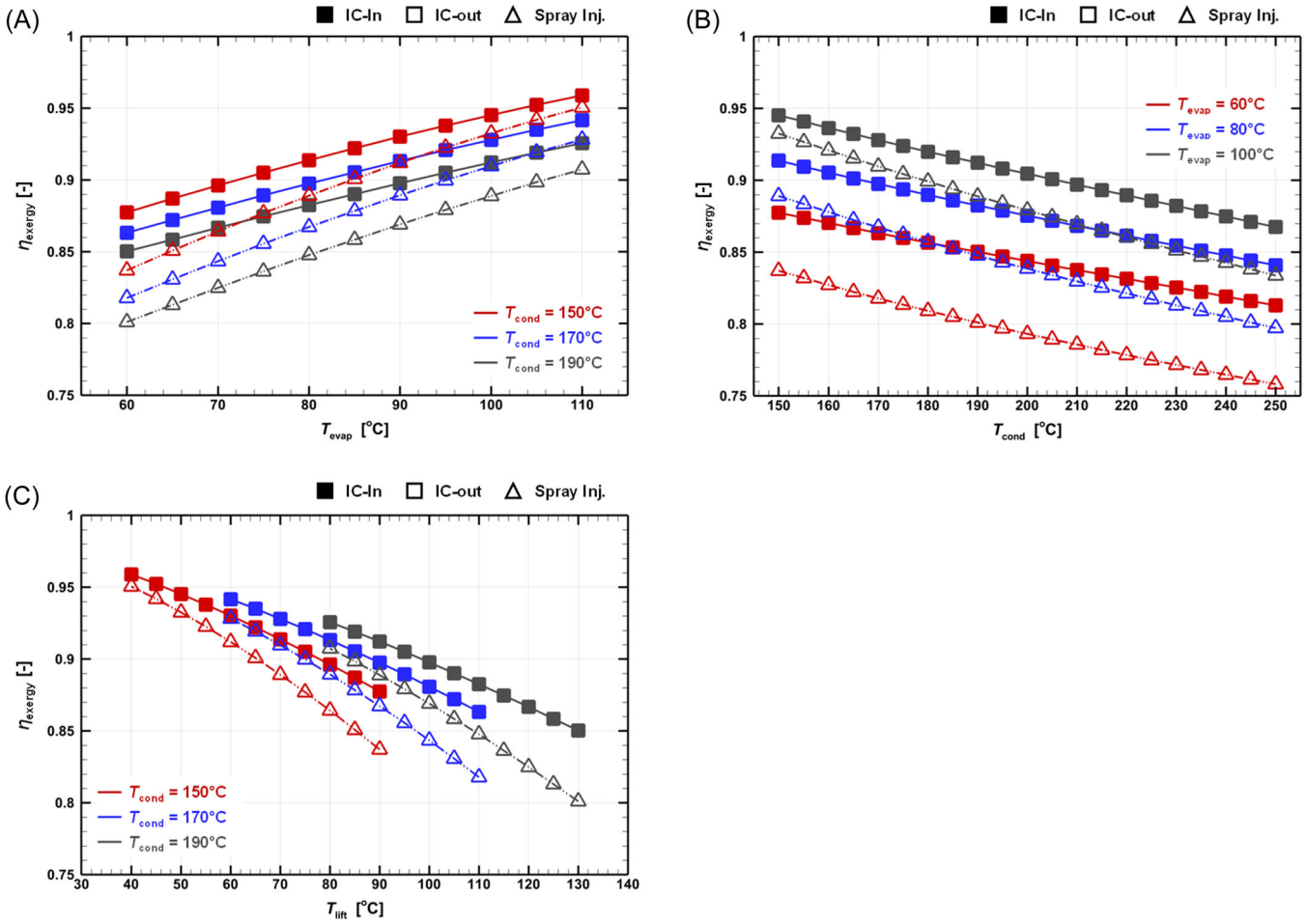

FIGURE 7 Exergy efficiency, η_{exergy}, changes according to (A) evaporation temperature, T_{evap}, (B) condensation temperature, T_{cond}, and (C) temperature lift, T_{lift}. IC, intercooler.

spray-injection cycle showed lower values. Similar to the results of the φ analysis, the overall η_{exergy} decrease as T_{lift} increases.

The η_{exergy} difference between the IC cycles and spray-injection change is also like that in the φ analysis. When the cycle has a T_{evap} of 60°C, the IC cycles have an η_{exergy} of 0.85–0.88 and the spray-injection cycle has 4.61%–6.79% lower exergy efficiency, and this difference has been reduced to 0.88%–1.97% with increasing T_{evap} to 110°C, Figure 7A. In addition, the discrepancy increased from 1.35%–4.61% to 3.89%–6.75% during T_{cond} increasing from 150°C to 250°C, Figure 7B. In terms of the η_{exergy} changes according to the temperature lift, Figure 7C, the differences between IC and spray-injection cycles are smaller compare to φ analysis. This difference was due to different evaluation subjects. While the φ analysis focused on the heat sink flow and its direct connection to demand, η_{exergy} analysis was conducted for the main cycle to evaluate the completeness of proposed heat pump cycles. The results of both analyses showed that IC cycles had higher COP and η_{exergy} values compared with the spray-injection cycle, indicating that IC cycles exhibit higher efficiency and systemic perfection.

3.3 | Practical performance of the HTHP cycles and CO_2 saving potential

The technical feasibility of the Rankine cycle using steam compression equipment is demonstrated for HTHPs, and turbo compressors are considered to be a promising solution.[22,34] To understand the practical performance of the proposed HTHP cycles, the COP and $T_{sink\ out}$ were investigated, Figure 8. The PR per compression stage of the turbo compressor using water vapor is expected to reach up to 3.5.[35,36] However, considering its efficiency, the practical PR was assumed to <2.5.

The analysis revealed that the available temperature lift is limited to approximately 60–65 K when PR < 2.5 for each stage. Specifically, the IC-in cycle was found to demonstrate higher COP and $T_{sink\ out}$ values compared

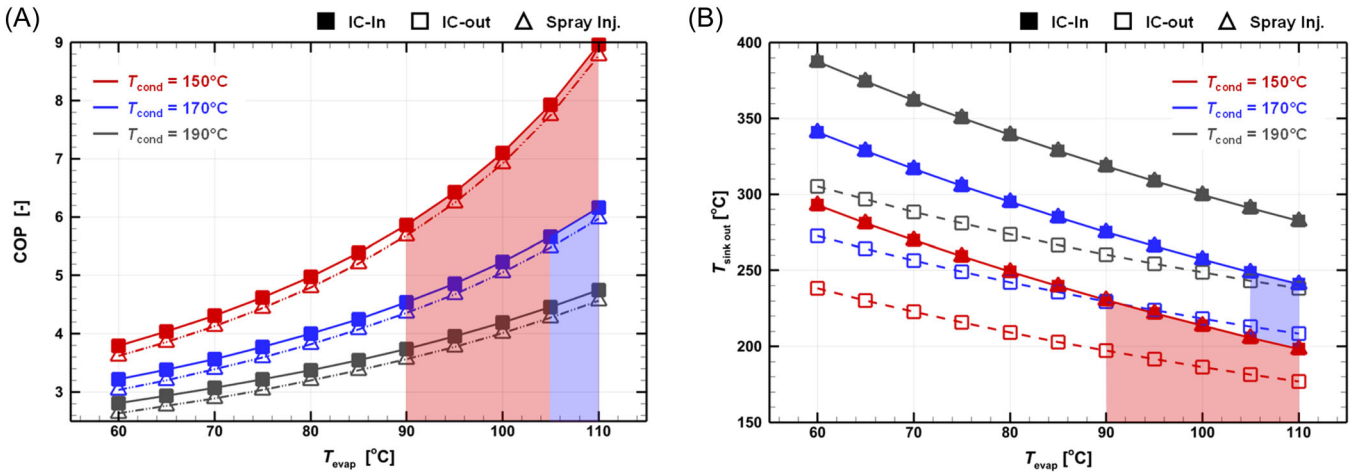

FIGURE 8 Estimated practical performance of the HTHP cycles by considering practical pressure ratio: (A) COP and (B) $T_{sink\ out}$ by T_{evap}. COP, coefficient of performance; HTHP, high-temperature heat pump; IC, intercooler.

TABLE 3 CO_2 emission intensities for different energy sources and CO_2 savings potential.

Thermal energy (conventional)			Electrical energy (HTHP)			
Source	CO_2 intensity (g/kWh_{th})	CO_2 emission (Mt/year)	Source	CO_2 intensity (g/kWh_{el})	CO_2 emission (Mt/year)	CO_2 reduction (%)
Oil	270.7	138.6	EU 2021	275.0	24.0	81.2
Natural gas	235.6	120.6	EU 2030	118.0	10.3	91.9
LPG	272.9	139.7				

Abbreviations: EU, European Union; HTHP, high-temperature heat pump; LPG, liquefied petroleum gas.

with the spray-injection cycle and IC-out cycle, respectively, due to its cycle architectural characteristics as previously discussed. The IC-in cycle was able to achieve a COP of 5.86, equivalent to 720 kW, and a $T_{sink\ out}$ of over 200°C when the cycle's T_{evap} and T_{cond} are set to 90°C and 150°C.

On the basis of the above results, it is possible to estimate the amount of energy saving and the reduction in CO_2 emissions achieved through the application of the proposed HTHP system. According to data from 2012, the final energy consumption in the industrial sector of EU28 was 3200 TWh, with process heating accounting for 60% of this total (1920 TWh). In addition, the target temperature range of this study is 100–200°C, which corresponds to approximately 16% (512 TWh) of the total energy demand. This energy is mostly required by the pulp and paper industry, and other nonclassified subsectors.[7]

The GHG emission intensity for different fossil boilers and electricity generation in Europe, along with the CO_2 saving potential are listed in Table 3. Conventional fossil boilers have CO_2 emission intensities of ~250 g CO_2-eq/kWh_{th}, while electricity generation in the EU had an emission intensity of 275.0 g CO_2-eq/kWh_{el} in 2021, which is projected to reduce to 118.0 g CO_2-eq/kWh_{el} by 2030.[37,38] By substituting existing fossil boilers with a highly efficient HTHP system, there will be a significant reduction in total energy consumption. The HTHP showed a COP of 5.86 with $T_{sink\ out}$ exceeding 200°C under 90–150 conditions in Figure 8. This result indicates that electrification can significantly reduce the amount of CO_2 emission from industrial processes operating between 100°C and 200°C. The CO_2 emission intensity is estimated to decrease from approximately 128 to 24.0 Mt/year in 2021, and further decrease to 10.3 Mt by 2030. The HTHP system for industrial processes has the potential to reduce net GHG emissions by up to 8.1% in 2030, compared with conventional fossil boilers (~250 g CO_2-eq/kWh_{th}). Overall, the HTHP system is a promising option for reducing energy consumption in industrial processes and decreasing CO_2 emissions in various ways.

4 | CONCLUSION

HTHP cycles with three different intercooling strategies have been proposed to supply high-temperature thermal energy (>200°C) for industrial processes. These include two IC cycles with different directions of heat sink flow and one spray-injection cycle.

As the temperature lift increases, there is a decrease in the overall COP and m_{sink} values, accompanied by an increase in $T_{sink\ out}$ values. The IC-in cycle exhibits the higher COP and $T_{sink\ out}$ values compare to the spray-injection and IC-out cycles, respectively. The highest COP was observed when both compressors had the same PR per stage, $PR_1/PR_2 = 1.0$, which was defined as the optimized PR. From the thermodynamic and exergy efficiency analysis at the optimized PR, it was confirmed that the overall φ and η_{exergy} increased as the temperature lift decreased. The spray-injection cycle consistently showed lower φ and η_{exergy} values than the IC cycles due to limitations in cycle architecture. Especially, the IC-in cycle, with a T_{evap} of 60°C and T_{cond} of 150°C, achieved a COP of approximately 5.86 and $T_{sink\ out}$ of over 200°C when the practical PR per stage ($PR < 2.5$) was applied.

In conclusion, the proposed multistage HTHP cycles have the potential to provide high-temperature thermal energy (>200°C) for industrial processes with high efficiency. Moreover, its application is expected to reduce CO_2 emissions from industrial processes up to 200°C by 91.9% compared with conventional fossil boilers in 2030. The HTHP systems can significantly contribute to achieving Low-Carbon Industrial Processes and a sustainable energy transition.

NOMENCLATURE

E	exergy (kW)
h	specific enthalpy (kJ/kg)
m	mass flow rate (kg/s)
P	pressure (bar)
Q	energy (kW)
s	specific entropy (kJ/kg K)
T	temperature (°C or K)
W	power (kW)

GREEK SYMBOLS

η	exergy efficiency (dimensionless)
ε	specific exergy (kJ/kg)
φ	thermodynamic efficiency (dimensionless)

SUBSCRIPTS

0	ambient conditions
1	first compression stage
2	second compression stage
carnot	Carnot
cond	condenser
exergy	exergy
evap	evaporator
in	Inlet
inj	injection flow
int	intermediate
main	main cycle
out	outlet
sink	heat sink
sub	subcooling
sup	superheating

ACKNOWLEDGMENTS

Open Access funding enabled and organized by Projekt DEAL.

ORCID

Seon Tae Kim http://orcid.org/0000-0002-4388-3996

REFERENCES

1. Crippa M, Guizzardi D, Solazzo E, et al. *GHG emissions of all world countries—2021 report*; Publications Office of the European Union. 2021.
2. Lamb WF, Wiedmann T, Pongratz J, et al. A review of trends and drivers of greenhouse gas emissions by sector from 1990 to 2018. *Environ Res Lett*. 2021;16(7):073005.
3. Edenhofer O, ed. *Climate Change 2014: Mitigation of Climate Change Working Group III contribution to the Fifth Assessment Report of the Intergovernmental Panel on Climate Change*. Cambridge University Press; 2014.
4. IEA. *Key World Energy Statistics 2021*; 2021.
5. European Commission. *EU Reference Scenario 2016: Energy, Transport and GHG emissions Trends to 2050*; 2016.
6. Eurostat. *Energy Balances 2019*. Accessed February 28, 2022. https://ec.europa.eu/eurostat/web/energy/data/energy-balances
7. Tobias F, Steinbach J, Ragwitz M, et al. *Mapping and Analyses of the Current and Future (2020–2030) Heating/Cooling Fuel Deployment (Fossil/RenEwables) Work Package 1: Final Energy Consumption for the Year 2012 Final Report: 54296* (Technical report). 2016. https://doi.org/10.13140/RG.2.2.29193.75361
8. Marina A, Spoelstra S, Zondag HA, Wemmers AK. An estimation of the European industrial heat pump market potential. *Renewable Sustainable Energy Rev*. 2021;139:110545.
9. Simon P, Stefano Z, Silvia C, et al. *D2.3 WP2 Report—Open Data Set for the EU28* (Technical report). 2018. https://www.hotmaps-project.eu/wp-content/uploads/2018/03/D2.3-Hotmaps_for-upload_revised-final_.pdf
10. Huang F, Zheng J, Baleynaud JM, Lu J. Heat recovery potentials and technologies in industrial zones. *J Energy Inst*. 2017;90(6):951-961.

11. Brueckner S, Miró L, Cabeza LF, Pehnt M, Laevemann E. Methods to estimate the industrial waste heat potential of regions—a categorization and literature review. *Renewable Sustainable Energy Rev*. 2014;38:164-171.
12. Tauveron N, Colasson S, Gruss J-A. Available systems for the conversion of waste heat to electricity. In: *Energy*. Vol 6A. American Society of Mechanical Engineers; 2014:1114. https://doi.org/10.1115/IMECE2014-37984
13. Wolf S, Blesl M, eds. Model-Based Quantification of the Contribution of Industrial Heat Pumps to the European Climate Change Mitigation Strategy. *ECEEE Industrial summer study proceedings*. 2016. https://www.eceee.org/library/conference_proceedings/eceee_Industrial_Summer_Study/2016/4-technology-products-and-systems/model-based-quantification-of-the-contribution-of-industrial-heat-pumps-to-the-european-climate-change-mitigation-strategy/
14. Brückner S, Liu S, Miró L, Radspieler M, Cabeza LF, Lävemann E. Industrial waste heat recovery technologies: an economic analysis of heat transformation technologies. *Appl Energy*. 2015;151:157-167.
15. Hammond GP, Norman JB. Heat recovery opportunities in UK industry. *Appl Energy*. 2014;116:387-397.
16. Lauterbach C, Schmitt B, Jordan U, Vajen K. The potential of solar heat for industrial processes in Germany. *Renewable Sustainable Energy Rev*. 2012;16(7):5121-5130.
17. Martin P, Jan B, Marlene A, Farikha I, Eberhard J, eds. *Industrial Waste Heat—Tapping into a Neglected Efficiency Potential. ECEEE Industrial summer study proceedings*. 2011. https://www.eceee.org/library/conference_proceedings/eceee_Summer_Studies/2011/3-energy-use-in-industry-the-road-from-policy-to-action/industrial-waste-heat-tapping-into-a-neglected-efficiency-potential/
18. Chua KJ, Chou SK, Yang WM. Advances in heat pump systems: a review. *Appl Energy*. 2010;87(12):3611-3624.
19. Chamoun M, Rulliere R, Haberschill P, Peureux J-L. Experimental and numerical investigations of a new high temperature heat pump for industrial heat recovery using water as refrigerant. *Int J Refrig*. 2014;44:177-188.
20. German Energy Agency (DENA). *Process Heat in Industry and Commerce: Technology Solutions for Waste Heat Utilisation and Renewable Provision*; 2016.
21. van de Bor DM, Infante Ferreira CA. Quick selection of industrial heat pump types including the impact of thermodynamic losses. *Energy*. 2013;53:312-322.
22. Arpagaus C, Bless F, Uhlmann M, Schiffmann J, Bertsch SS. High temperature heat pumps: market overview, state of the art, research status, refrigerants, and application potentials. *Energy*. 2018;152:985-1010.
23. Schulz M, Kourkoulas D. Regulation (EU) No 517/2014 of The European Parliament and of the council of 16 April 2014 on fluorinated greenhouse gases and repealing Regulation (EC) No 842/2006. *Off J Eur Union*. 2014;517:L150.
24. Liu H, Xiao H. Study on performances of refrigeration-type compressed-air dryers using environmentally-friendly refrigerants R717, R290 and R600a. *AMM*. 2014;672-674:1708-1711.
25. Nawaz K, Shen B, Elatar A, Baxter V, Abdelaziz O. R290 (propane) and R600a (isobutane) as natural refrigerants for residential heat pump water heaters. *Appl Therm Eng*. 2017;127:870-883.
26. Wu D, Jiang J, Hu B, Wang RZ. Experimental investigation on the performance of a very high temperature heat pump with water refrigerant. *Energy*. 2020;190:116427.
27. Dai B, Qi H, Liu S, et al. Environmental and economical analyses of transcritical CO2 heat pump combined with direct dedicated mechanical subcooling (DMS) for space heating in China. *Energy Convers Manage*. 2019;198:111317.
28. Agrawal N, Bhattacharyya S. Studies on a two-stage transcritical carbon dioxide heat pump cycle with flash intercooling. *Appl Therm Eng*. 2007;27(2-3):299-305.
29. STEAG Energy Services GmbH. *EBSILON Professional*; 2020.
30. Yağlı H, Koç Y, Kalay H. Optimisation and exergy analysis of an organic Rankine cycle (ORC) used as a bottoming cycle in a cogeneration system producing steam and power. *Sustainable Energy Technol Assess*. 2021;44:100985.
31. Ye X, Dong Z, Lu J, Li C. Thermoeconomic evaluation of double-reheat coal-fired power units with carbon capture and storage and waste heat recovery using organic Rankine cycle. *Int J Greenhouse Gas Control*. 2021;105:103247.
32. Szargut J. Component efficiencies of a vapour-compression heat pump. *Exergy Int J*. 2002;2(2):99-104.
33. Kabul A, Kizilkan Ö, Yakut AK. Performance and exergetic analysis of vapor compression refrigeration system with an internal heat exchanger using a hydrocarbon, isobutane (R600a). *Int J Energy Res*. 2008;32(9):824-836.
34. Zühlsdorf B, Bühler F, Bantle M, Elmegaard B. Analysis of technologies and potentials for heat pump-based process heat supply above 150°C. *Energy Convers Manage X*. 2019;2:100011.
35. Šarevski MN, Šarevski VN. Thermal characteristics of high-temperature R718 heat pumps with turbo compressor thermal vapor recompression. *Appl Therm Eng*. 2017;117:355-365.
36. Šarevski MN, Šarevski VN. Characteristics of water vapor turbocompressors applied in refrigeration and heat pump systems. *Int J Refrig*. 2012;35(5):1484-1496.
37. Casasso A, Capodaglio P, Simonetto F, Sethi R. Environmental and economic benefits from the phase-out of residential oil heating: a study from the Aosta Valley Region (Italy). *Sustainability*. 2019;11(13):3633.
38. European Environment Agency. Greenhouse gas emission intensity of electricity generation in Europe. In: *The CO_2 Emission Intensity is Calculated as the ratio of CO_2 Emissions from Electricity Generation and Gross Electricity Generation*. https://www.eea.europa.eu/ims/greenhouse-gas-emission-intensity-of-1

How to cite this article: Kim ST, Hegner R, Özuylasi G, Stathopoulos P, Nicke E. Performance analysis of multistage high-temperature heat pump cycle. *Energy Sci Eng*. 2023;1-12. doi:10.1002/ese3.1536